Electron transport from a one-dimensional lead to a two-dimensional graphene sheet through a single site

2008 J. Phys.: Condens. Matter 20 055207

(http://iopscience.iop.org/0953-8984/20/5/055207)

IOP PUBLISHING JOURNAL OF PHYSICS: CONDENSED MATTER

J. Phys.: Condens. Matter **20** (2008) 055207 (9pp) doi:10.1088/0953-8984/20/5/055207

Electron transport from a one-dimensional lead to a two-dimensional graphene sheet through a single site

Taturo Fukuda[1], **Hüseyin Oymak**[2] **and Jongbae Hong**[3]

[1] Department of Physics, Tokai University, Kitakaname 1117, Hiratsuka, Kanagawa 259-1292, Japan
[2] BK21 Physics Program and Department of Physics, Chungbuk National University, Cheongju 361-763, Korea
[3] Department of Physics and Astronomy, Seoul National University, Seoul 151-747, Korea

E-mail: tfukuda@phya.snu.ac.kr and oymak@newton.physics.metu.edu.tr

Received 4 June 2007, in final form 7 November 2007
Published 17 January 2008
Online at stacks.iop.org/JPhysCM/20/055207

Abstract

The problem of electron transport through a graphene-based device is studied theoretically and numerically. The device is composed of a single central site, with a single energy level, which is connected to a one-dimensional lead, and a two-dimensional graphene sheet. The nonequilibrium Green function formalism is utilized in modeling the problem; the formulation and numerical calculations are carried out around a K-point, in the band structure of the graphene, where the Fermi energy is located. Particular importance is placed on the transmission and current–voltage (I–V) characteristics of the device under a small bias. We find that the graphene part causes the central transmission peak, originally due to the single energy level of the central site, to split into two peaks, leaving an anti-resonant, zero-transmission, dip between them; only one of these peaks contributes to the resultant current. There always appears an almost flat, practically zero-current, region on a rather large bias interval, centered around the Fermi energy of the graphene, in the I–V graphs.

1. Introduction and the model studied

Perhaps beginning from the work of Wallace [1], graphene, a single layer of carbon atoms packed densely into a honeycomb structure, has played the key role in investigating the properties of numerous carbon-based materials such as graphite, fullerenes, nanotubes, etc [2]. Although until very recently they were reckoned to be unstable, and therefore not to exist, in 2004 Novoselov *et al* [3, 4] managed to obtain very thin graphitic sheets, and even a single layer of graphene sheet. This achievement has opened up new possibilities to fabricate many novel submicron-devices from graphene sheet due to its unprecedented versatility. They reported that the graphitic films have turned out to be of very high crystal quality, (semi)metallic, continuous on a macroscopic scale, and, most importantly, stable under ambient conditions. They pointed out that electronic transport in such a two-dimensional (2D) film would be ballistic at submicrometer distances. It was observed in a later experimental study [5] that the conductivity of graphene never falls below a minimum, no matter how small the concentrations of charge carriers are.

Electronic properties of graphene are markedly different from those of conventional 2D materials such as a metal surface, GaAs/GaAlAs superlattice, surface of liquid helium 4, etc [6, 7]. The difference is caused primarily by the unique band structure of graphene, in which the conduction and valance bands osculate at two (inequivalent) hexagonal Brillouin zone corners, called the K-, or Dirac, point. At low energies the 2D energy dispersion relation of graphene can be shown to be linear. It has been shown that it is the Dirac's relativistic equation (also called the Weyl equation) that governs the dynamics of the electron transport in graphene at low energies, for the charge carriers in graphene, with their zero rest-mass, imitate relativistic particles and have an effective 'speed of light' of the order of 10^6 m s^{-1} [5, 6]. Graphene's unusual properties make graphene-based materials, as opposed to silicon-based ones, so promising that they are expected to be the new

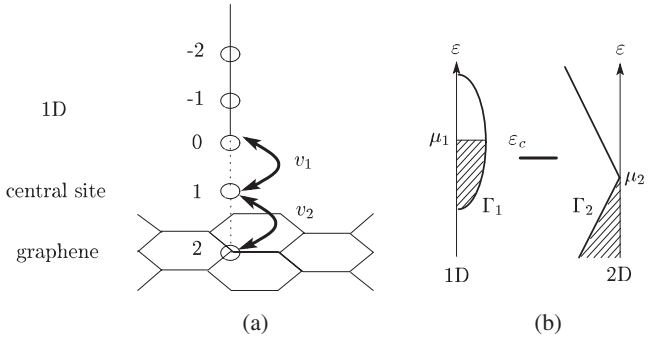

Figure 1. (a) The system under study. (b) The energy-band diagram for the system in which the voltage bias is $eV > 0$. The left (right) side is for the LDOS of the 1D (2D) part; the bold line in the middle is for the energy level of the central site.

foundation stone for the near future submicron electronic devices [8–10].

In this work we deal with the problem of electron transport through a graphene-based mesoscopic device. The *system* that we consider within the nearest-neighbor tight-binding scheme is composed of a semi-infinite 1D lead with the hopping energy t_1, an infinitely-large 2D graphene layer with t_2, and between and coupled to them a single site with the on-site energy ε_c, as is depicted in figure 1(a). The system is biased at a voltage V, at low temperature, by an external source–drain mechanism which is in contact with the 1D and 2D parts (not shown). Our purpose is to investigate the transmission properties and the current–voltage (I–V) characteristics of such a device. Envisaging the 1D lead being the tip part, the system under consideration might be regarded as a simple model to study an adatom on a 2D graphene sheet in a scanning tunneling microscopy (STM) experiment. By laying down the rudiments of such a simple system, our principle aim is to provide valuable insights into similar but more complicated systems which are expected to be commonplace in the not-too-distant future.

The presence of an external bias requires that the device be treated as a nonequilibrium system. The tunneling current through such a system has been derived by Caroli *et al* [11] by means of the nonequilibrium Green function (NEGF) formalism invented by Keldysh [12]. In this work we also make use of Caroli's well established formulation to explore especially the effects of the 2D graphene part on the transport properties of the system.

2. Formulation

The total Hamiltonian associated with the system in figure 1(a) is

$$H = H_1 + H_2 + H_c + H_T \tag{1}$$

where

$$H_1 = \mu_1 \sum_j c_j^\dagger c_j - t_1 \sum_{\langle j,i\rangle} c_j^\dagger c_i, \tag{2}$$

$$H_2 = \mu_2 \sum_j a_j^\dagger a_j - t_2 \sum_{\langle j,i\rangle} a_j^\dagger a_i, \tag{3}$$

$$H_c = \varepsilon_c d_1^\dagger d_1, \tag{4}$$

$$H_T = (v_1 c_0^\dagger d_1 + v_2 a_2^\dagger d_1) + \text{H.c.} \tag{5}$$

Here H_1, H_2, and H_c are the respective Hamiltonians describing the electron motion in the 1D, 2D, and central parts. We assume that the electrochemical potentials of the 1D and 2D parts, μ_1 and μ_2, respectively, do not depend on the site indices, and that the two atoms in the graphene unit cell are treated as identical. The potential difference between the 1D and 2D parts is related to the applied voltage bias as $\mu_1 - \mu_2 = eV$. The usual creation operators for the electron in the 1D, 2D, and central parts are respectively designated by $c_j^\dagger$, $a_j^\dagger$, and $d_1^\dagger$, which satisfy the anti-commutation relations $\{c_i, c_j^\dagger\} = \delta_{ij}$, $\{a_i, a_j^\dagger\} = \delta_{ij}$, and $\{d_1, d_1^\dagger\} = 1$. The transfer Hamiltonian H_T describes the electron hopping between the central site and the 1D and 2D parts. The hopping energies between sites $j = 0$ and 1 and between $j = 1$ and 2 are given by v_1 and v_2, respectively.

As the form of total Hamiltonian (1) suggests, in this work we neglect the electron–phonon and the phonon mediated electron–phonon interactions due to the 2D graphene part, and the Coulomb interaction at the central site. We assume that a gate is coupled to the central site so intimately that the single energy level ε_c is unchanged by the source–drain mechanism and is kept constant all the time. We also take the hopping energies v_1 and v_2 to be constant by assuming that the single electron charging energy associated with the central site is at most comparable to $k_B T$, where T is temperature. In this respect temperature in this work is assumed to be sufficiently small to exclude all the temperature-dependent effects, but sufficiently high to just avoid the Coulomb blockade regime, because our aim in this study is to focus on the effects due largely to the special band structure of graphene.

In Caroli's treatment the transfer Hamiltonian H_T is regarded as a perturbation, and the steady current through the system is expressed as [11]

$$I = \frac{4e}{h} \int_{-\infty}^{\infty} \mathrm{d}\varepsilon |G_{11}^r(\varepsilon)|^2 \Gamma_1(\varepsilon)\Gamma_2(\varepsilon) \times [f(\varepsilon - \mu_1) - f(\varepsilon - \mu_2)], \tag{6}$$

where $f(\varepsilon - \mu_i) = 1/\{1 + \exp[\beta(\varepsilon - \mu_i)]\}$, with $\beta = 1/k_B T$, is the Fermi–Dirac distribution function for the 1D and 2D parts. The functions

$$\Gamma_1(\varepsilon) = \pi |v_1|^2 \rho(j, \varepsilon)\Big|_{j=0} \quad \text{and} \quad \Gamma_2(\varepsilon) = \pi |v_2|^2 \rho(j, \varepsilon)\Big|_{j=2} \tag{7}$$

are related respectively to the tunneling rate between the central site and the 1D and 2D parts, with

$$\rho(j, \varepsilon) = -\operatorname{Im} g_{jj}^r(\varepsilon)/\pi \tag{8}$$

being the local density of states (LDOS) at site j, where g_{jj}^r is the unperturbed retarded Green function for 1D and/or 2D parts. Finally in equation (6) is the full retarded Green function, $G_{11}^r(\varepsilon)$, for the central site whose calculation is

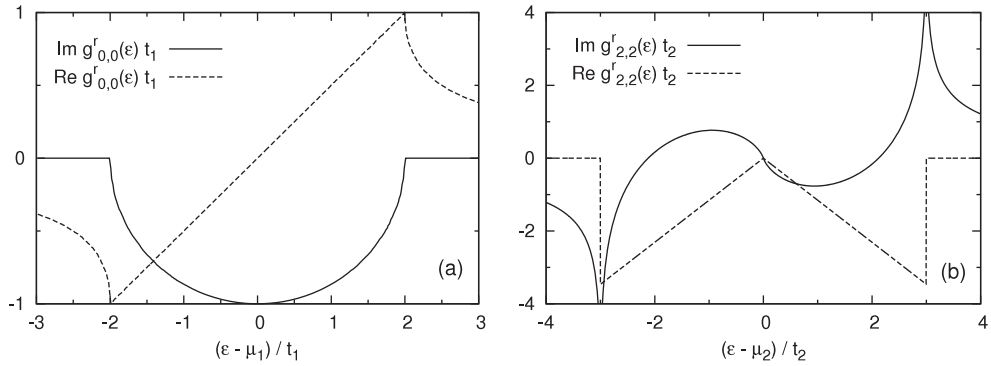

Figure 2. Plots of the real and imaginary parts of (a) $g^r_{00}(\varepsilon)$, given by equations (10) and (11), and (b) $g^r_{22}(\varepsilon)$, given by equations (18) and (19).

carried out in the presence of the coupling of the central site to the 1D and 2D parts, and it follows from the Keldysh Green function technique [12] as

$$G^r_{11}(\varepsilon) = [1 - |v_1|^2 g^r_{11}(\varepsilon) g^r_{00}(\varepsilon) - |v_2|^2 g^r_{11}(\varepsilon) g^r_{22}(\varepsilon)]^{-1} g^r_{11}(\varepsilon), \tag{9}$$

which has the same form as that in Caroli's work [11]. This result expresses the level broadening effect (the broadening of the single discrete energy level ε_c into a continuous density of states) which comes unavoidably with the coupling of the central site, $j = 1$, to the 1D and 2D parts; we later expound more on this.

As equations (6)–(9) imply, the unperturbed Green functions for the 1D, 2D, and central parts are the key ingredients in the calculation of any quantity of interest for the system under consideration. The real and imaginary parts of the edge Green function $g^r_{00}(\varepsilon)$ for the 1D part have been calculated in a previous work of ours [13]:

$$\mathrm{Re}\, g^r_{00}(\varepsilon) = \frac{1}{t_1}\left\{ \alpha(\varepsilon) - \mathrm{sgn}[\alpha(\varepsilon)]\theta[\alpha(\varepsilon)^2 - 1] \times \sqrt{\alpha(\varepsilon)^2 - 1}\right\}, \tag{10}$$

$$\mathrm{Im}\, g^r_{00}(\varepsilon) = -\frac{1}{t_1}\theta[1 - \alpha(\varepsilon)^2]\sqrt{1 - \alpha(\varepsilon)^2}, \tag{11}$$

where $\alpha(\varepsilon) = (\varepsilon - \mu_1)/2t_1$. The graphs of equations (10) and (11) are plotted in figure 2(a). The LDOS at the edge site, $\rho(j, \varepsilon)|_{j=0}$, possesses a semi-elliptic shape with a bandwidth of $4t_1$. The reader is to notice that these results are essentially the same as those in the chemisorption theory [14–17].

The usual Fourier transform of $\mathrm{i}g^r_{11}(t) = \theta(t)\langle\{d_1(t), d_1^\dagger(0)\}\rangle$ gives the Green function $g^r_{11}(\varepsilon)$ for the isolated central site as

$$g^r_{11}(\varepsilon) = 1/(\varepsilon - \varepsilon_c + \mathrm{i}0^+). \tag{12}$$

As to the 2D graphene part, we choose the xy-plane to be parallel to that of the graphene; the eigenvalues associated with the unperturbed Hamiltonian (3) are then obtained as [1, 2]

$$\varepsilon_{s\mathbf{q}} = \mu_2 + st_2\left[1 + 4\cos\left(\frac{3a}{2}q_x\right)\cos\left(\frac{\sqrt{3}a}{2}q_y\right) + 4\cos^2\left(\frac{\sqrt{3}a}{2}q_y\right)\right]^{1/2}, \tag{13}$$

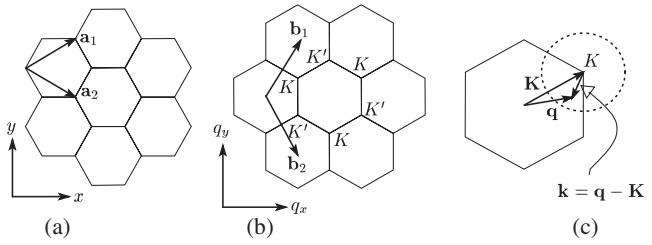

Figure 3. (a) The direct lattice of graphene, and (b) its reciprocal lattice; $\mathbf{a}_i$ and $\mathbf{b}_i$ are the respective basis vectors. Also given in (c) is the first Brillouin zone, where the radius of the dotted circle is k_c.

where $s = +1$ (-1) is for the conduction (valence) band, and a is the lattice constant in the real space. We next write the Fourier transform of the unperturbed Green function for the graphene at site 2, i.e., $\mathrm{i}g^r_{22}(t) = \theta(t)\langle\{a_2(t), a_2^\dagger(0)\}\rangle$, with the annihilation operator, $a_2 = \frac{1}{\sqrt{\mathcal{N}}}\sum_{\mathbf{q}} \mathrm{e}^{\mathrm{i}\mathbf{q}\cdot\mathbf{r}_2} a_{\mathbf{q}}$, where $\mathcal{N}$ is the number of unit cells to be included in the calculation:

$$g^r_{22}(\varepsilon) = \frac{1}{\mathcal{N}}\sum_{s=\pm1}\sum_{q_1=-\mathcal{N}_1/2}^{\mathcal{N}_1/2}\sum_{q_2=-\mathcal{N}_2/2}^{\mathcal{N}_2/2}\frac{1}{\varepsilon - \varepsilon_{s\mathbf{q}} + \mathrm{i}0^+}, \tag{14}$$

where $\mathcal{N} = \mathcal{N}_1\mathcal{N}_2$, and q_1 and q_2 are the components of the wavevector $\mathbf{q}$ along the reciprocal basis vectors, see figure 3(b): $\mathbf{q} = q_1\mathbf{b}_1 + q_2\mathbf{b}_2 = q_x\mathbf{e}_x + q_y\mathbf{e}_y$. For large $\mathcal{N}$ the discrete summations in equation (14) over q_1 and q_2 can be cast down to an integral over the first Brillouin zone (FBZ); the result is

$$g^r_{22}(\varepsilon) = \frac{1}{\Omega^*}\sum_{s=\pm1}\int\int_{\mathrm{FBZ}}\frac{\mathrm{d}q_x\,\mathrm{d}q_y}{\varepsilon - \varepsilon_{s\mathbf{q}} + \mathrm{i}0^+}, \tag{15}$$

where Ω^* is the area of the FBZ which is related to the area $\Omega = 3\sqrt{3}a^2/2$ of the unit cell of the real space via $\Omega\Omega^* = (2\pi)^2$.

In this work we focus on the transport properties of the electrons possessing a momentum only in the immediate vicinity of a K-point in the FBZ with a wavevector $\mathbf{K}$; see figure 3(b). Consequently, it suffices to Taylor expand equation (13) around such a K-point. The result is a linear energy dispersion relation [1, 2]

$$\varepsilon_{sk} \simeq \mu_2 + s\gamma k \qquad \text{for } ka \ll 1, \tag{16}$$

where $\mathbf{k}$ is measured from a K-point as $\mathbf{k} = \mathbf{q} - \mathbf{K}$, $k = |\mathbf{k}|$, and $\gamma = 3at_2/2$ is the so-called effective 'speed of light'. In this approximation, the integral in equation (15) can be taken as

$$g^r_{22}(\varepsilon) \simeq \frac{1}{\Omega^*} \sum_{s=\pm 1} \int\int_{\text{near}\,K} \frac{\mathrm{d}k_x\,\mathrm{d}k_y}{\varepsilon - \varepsilon_{sk} + \mathrm{i}0^+}$$
$$= \frac{2}{\Omega^*} \sum_{s=\pm 1} \int_0^{k_c} \int_0^{2\pi} \frac{k\,\mathrm{d}k\,\mathrm{d}\theta}{\varepsilon - \varepsilon_{sk} + \mathrm{i}0^+},$$

so that

$$g^r_{22}(\varepsilon) = \frac{\Omega}{\pi} \sum_{s=\pm 1} \int_0^{k_c} \frac{k\,\mathrm{d}k}{\varepsilon - \mu_2 - s\gamma k + \mathrm{i}0^+}, \qquad (17)$$

where we have introduced, after Wang *et al* [18], a *cut-off momentum* k_c which is the radius of the circle centered at a K-point (see figure 3(c)), and is chosen in such a way that it is much smaller than the reciprocal lattice constant, i.e., $k_c \ll 4\pi/3a$. We then carry out the integral in equation (17) to get the real and imaginary parts of $g^r_{22}(\varepsilon)$ as

$$\mathrm{Re}\, g^r_{22}(\varepsilon) = \frac{\Omega(\varepsilon - \mu_2)}{\pi\gamma^2} \ln\left|1 + \frac{1}{(\varepsilon - \mu_2)^2/D^2 - 1}\right|, \qquad (18)$$

$$\mathrm{Im}\, g^r_{22}(\varepsilon) = -\frac{\Omega\,|\varepsilon - \mu_2|}{\gamma^2}\theta[1 - (\varepsilon - \mu_2)^2/D^2], \qquad (19)$$

where we have defined, for further convenience, $D = \gamma k_c$ as being the *cut-off energy*. The condition $k_c \ll 4\pi/3a$ then leads to $D \ll 2\pi t_2$. We choose $D/t_2 = 3.0$ throughout the present work, which is good enough to obtain all the important results presented in this work. In figure 2(b) are the graphs of equations (18) and (19). It follows from equations (8) and (19) that the LDOS at site 2 on the graphene possesses the renowned V-shaped feature around $\varepsilon = \mu_2$.

We note that Green functions (10)–(12), (18), and (19) depend in general on the applied bias voltage via the electrochemical potential of the 1D and 2D graphene parts, μ_1 and μ_2, respectively, and on the on-site energy of the central part, ε_c. In order to obtain the I–V characteristics of the system, the voltage profile should be determined from the outset. In the present work we adopt the symmetrical voltage profile shown in figure 1(b), which is given by

$$\mu_1 = eV/2, \qquad \mu_2 = -eV/2, \qquad \varepsilon_c = 0, \qquad (20)$$

where we have set the origin of energy as the Fermi energy at equilibrium. This profile seems most appropriate in describing the role of the 1D and graphene parts connected to an external source–drain mechanism, for both parts will then maintain a good number of electrons, necessary for a non-zero current, even under a small bias voltage.

3. Numerical results, discussions, and conclusions

Since at low temperature the Fermi–Dirac distribution function approaches the step function, i.e., $f(x) = [1 + \exp(x)]^{-1} \to \theta(-x)$, the general expression (6) for the tunneling current through the system is then reduced to, with the potential profile (20),

$$I(V) = \frac{e}{h} \int_{-eV/2}^{eV/2} \mathrm{d}\,\varepsilon \mathcal{T}(\varepsilon, V) \qquad (21)$$

with the transmission probability

$$\mathcal{T}(\varepsilon, V) = 4|G^r_{11}(\varepsilon)|^2 \Gamma_1(\varepsilon)\Gamma_2(\varepsilon) \qquad (22)$$
$$= \frac{4\Gamma_1(\varepsilon)\Gamma_2(\varepsilon)}{[\varepsilon - \Lambda_1(\varepsilon) - \Lambda_2(\varepsilon)]^2 + [\Gamma_1(\varepsilon) + \Gamma_2(\varepsilon)]^2}. \qquad (23)$$

Here the functions $\Lambda_1(\varepsilon)$ and $\Lambda_2(\varepsilon)$ are respectively defined by

$$\Lambda_1(\varepsilon) = |v_1|^2\,\mathrm{Re}\, g^r_{00}(\varepsilon) \qquad \text{and}$$
$$\Lambda_2(\varepsilon) = |v_2|^2\,\mathrm{Re}\, g^r_{22}(\varepsilon). \qquad (24)$$

Although the current expression (21), with (22), appears to possess the same form as that for a non-interacting region connected to two leads [11, 19, 20], we note some significant differences. Firstly, $G^r_{11}(\varepsilon)$ and $\Gamma_{1(2)}(\varepsilon)$ are voltage dependent; so is, in turn, the transmission probability (22). Consequently, a pure analytic study of the system under question is intractable; this is one of the reasons for why we, in this work, resort to a numerical calculation. Secondly, the tunneling rates of the 1D and graphene parts are not equal, i.e., $\Gamma_1(\varepsilon) \neq \Gamma_2(\varepsilon)$, so that they contribute differently to the transmission probability and current. In this respect, the present study provides a good opportunity to investigate the effect of 'leads' on the transmission properties of the system. Finally, the wide-band limit, which reduces the observable quantities of interest to simpler analytical forms [20], is not applicable to $\Gamma_2(\varepsilon)$, for it is not differentiable at $\varepsilon = \mu_2$; we can use the wide-band limit only for $\Gamma_1(\varepsilon)$ for small voltage biases. Remembering that we are interested especially in a K-point, i.e., in a small energy interval around $\varepsilon = \mu_2$, it would be nice if we could fully use the wide-band limit, at least to obtain some closed analytical results. But the situation without the wide-band limit in this work is not at all as adverse as it appears at first glance. As soon as we decide to use a numerical calculation, the present model is already capable of giving exact results, within the numerical accuracy used.

The transmission probability (22) has three ingredients: $\Gamma_{1(2)}(\varepsilon)$ and $G^r_{11}(\varepsilon)$. The former two convey to $\mathcal{T}(\varepsilon, V)$, via equations (7) and (8), the information about the LDOS at sites 0 and 2 so that they are exclusively pertaining to the 1D and 2D parts. The latter, $G^r_{11}(\varepsilon)$, on the other hand, performs two significant tasks. First, setting v_1 and v_2, which mediate the coupling of the 1D and 2D parts to the central site, equal to zero in equation (9), we obtain $G^r_{11}(\varepsilon)|_{v_1=v_2=0} = g^r_{11}(\varepsilon)$, equation (12). Therefore, $G^r_{11}(\varepsilon)$ contains the blueprint for the LDOS of the *isolated* central site. Second, it follows from equation (9) that $G^r_{11}(\varepsilon)$ also describes every possible path for the electron transport beginning from site 1 and ending again at site 1 in the *presence* of the 1D and 2D parts. In this sense $G^r_{11}(\varepsilon)$ plays one of the most crucial roles in this work; if we drew the graph of $|G^r_{11}(\varepsilon)|^2$, at zero voltage bias, we would see a peak around $\varepsilon = \varepsilon_c = 0$, corresponding in energy to the eigenvalue of the isolated central site. This peak would not be literally a delta function, corresponding to $|g^r_{11}(\varepsilon)|^2$, any more,

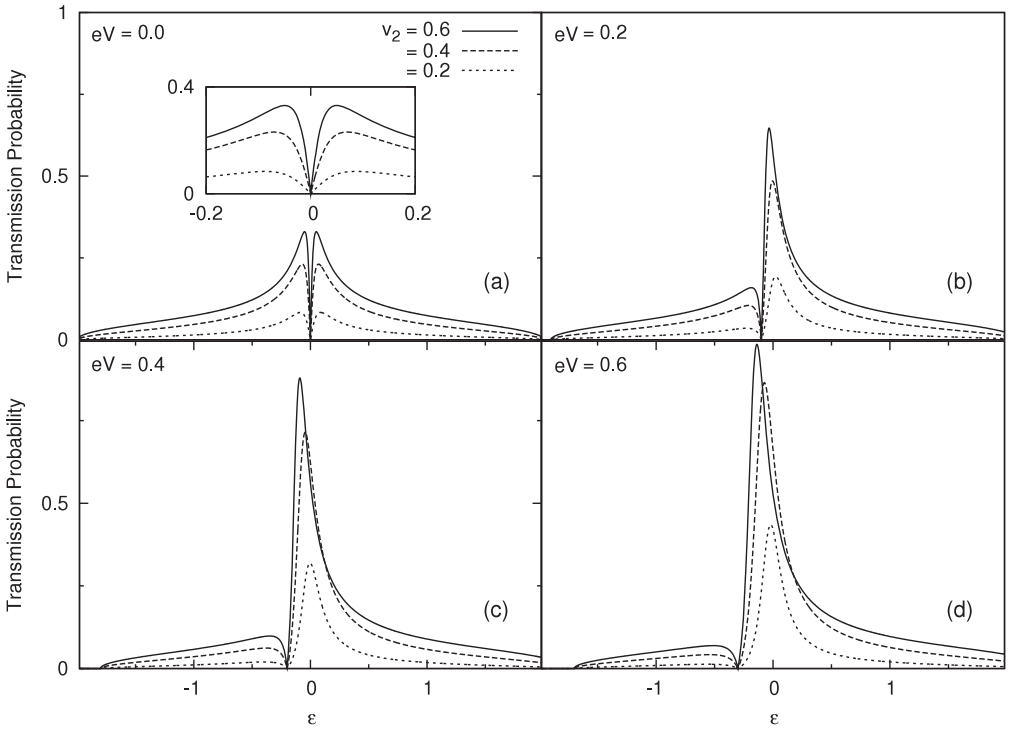

Figure 4. Transmission probability $\mathcal{T}(\varepsilon, V)$ for $v_1 = 0.3$. In the inset in (a) are the magnified portions of the same graphs around $\varepsilon = 0.0$.

as may be expected, because the coupling of the 1D and 2D parts to the central site results in a (level) broadening of the delta function, while reducing its height to some finite value.

We discuss briefly two prominent analytical properties of $\mathcal{T}(\varepsilon, V)$ which give in advance valuable insights into the evolution of the I–V characteristics of the system. We infer from the structures of the unperturbed Green functions that the transmission probability $\mathcal{T}(\varepsilon, V)$ does not change its analytic form on changing *simultaneously* the signs of ε and V, i.e.,

$$\mathcal{T}(-\varepsilon, -V) = \mathcal{T}(\varepsilon, V), \tag{25}$$

implying that under zero bias the transmission probability is symmetric around $\varepsilon = 0$, i.e., $\mathcal{T}(-\varepsilon, 0) = \mathcal{T}(\varepsilon, 0)$ (see figures 4(a) and 5(a) below). This suggests in turn that a non-zero bias always breaks this symmetry (see figures 4(b)–(d) and 5(b)–(d) below). A simple manipulation of the tunneling current (21) with the use of property (25) culminates in a current symmetric around $V = 0$, i.e., $I(-V) = -I(V)$ (see figure 6 below). We exploit this point in presenting our numerical results for the transmission probability by giving only the outcomes for positive bias voltages; the negative bias results will then be obvious.

Another noteworthy aspect of the transmission probability is that it vanishes at the electrochemical potential of the graphene part,

$$\mathcal{T}(-eV/2, V) = 0, \tag{26}$$

which follows directly from its definition (22) due to the special structure of $\Gamma_2(\varepsilon)$, closely related to the LDOS of the graphene, vanishing at $\varepsilon = \mu_2$; see the solid-line graph in figure 2(b). This feature is completely due to the 2D graphene part. The implication of this property is much more substantial and global than it may seem at first glance: no matter what the magnitude of the bias voltage V is, the transmission probability will be always zero at this special point, $\varepsilon = \mu_2 = -eV/2$ (see figures 4 and 5 below).

In figures 4–6 are shown sequentially the graphs of $\mathcal{T}(\varepsilon, V)$ and $I(V)$ for several combinations of the hopping energies v_1 and v_2. For convenience, we set t_1 as the energy scale. In figure 4, $\mathcal{T}(\varepsilon, V)$ is plotted for several voltage biases V, for various hopping energies v_2, keeping v_1 fixed at a non-zero value. All the graphs in this figure share the common structure in which there are two peaks, and between them is an anti-resonant (zero-transmission) dip located at $\varepsilon = -eV/2$. If we had considered a system composed of a single central site, and connected to which were two identical 1D left and right leads (i.e. if in the present system the 2D graphene part were replaced by a 1D lead), we would then have $\Gamma_1(\varepsilon) = \Gamma_2(\varepsilon)$ and see only one resonant peak around $\varepsilon = 0.0$, and no anti-resonant dip at all (see figure 7(a)). In the present system, however, $\Gamma_1(\varepsilon) \neq \Gamma_2(\varepsilon)$, and the inverse V-shape of $\Gamma_2(\varepsilon)$, with its apex at $\varepsilon = \mu_2 = 0.0$, leads to the peak–dip–peak structure in figure 4, and this is an effect coming purely from the 2D graphene part.

As is demonstrated in figures 4(a)–(d), as we increase the hopping energy v_2, keeping v_1 fixed, the heights of the two peaks increase gradually, irrespective of the bias voltage V. The increase in v_2 simply means the increase of the effect of the 2D graphene part on the system. This effect is combined in the transmission probability (22) via $\Gamma_2(\varepsilon)$ and $|G^r_{11}(\varepsilon)|^2$. Since the transmission probability is mainly dictated by the latter, it follows that, apart from the dip between the two peaks, the features of $\mathcal{T}(\varepsilon, V)$ are expected to be more and

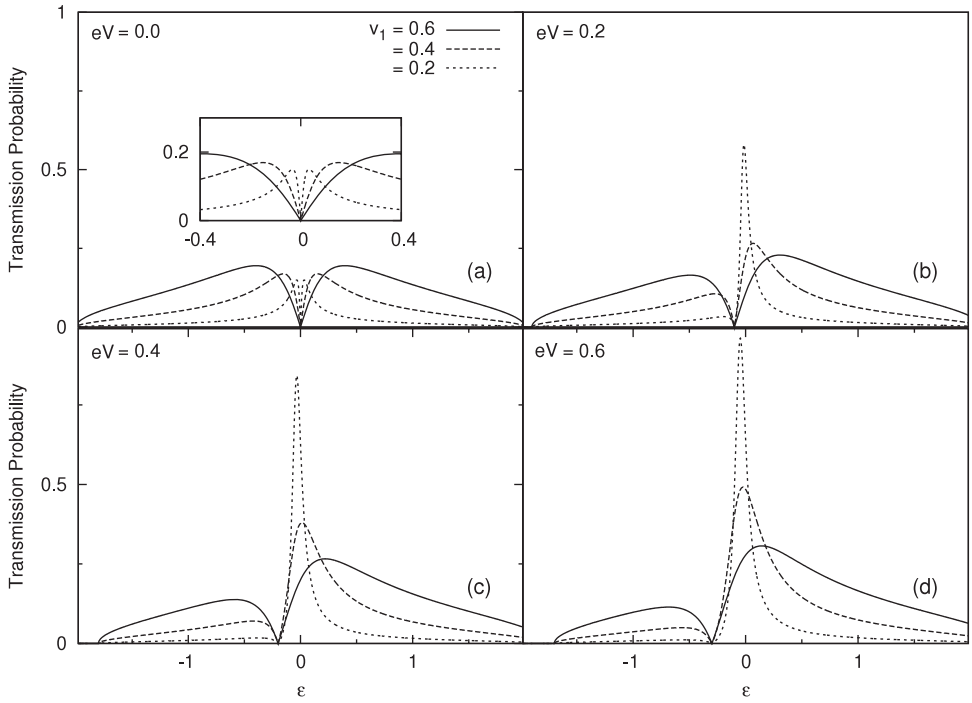

Figure 5. Transmission probability $\mathcal{T}(\varepsilon, V)$ for $v_2 = 0.3$. In the inset in (a) are the magnified portions of the same graphs around $\varepsilon = 0.0$.

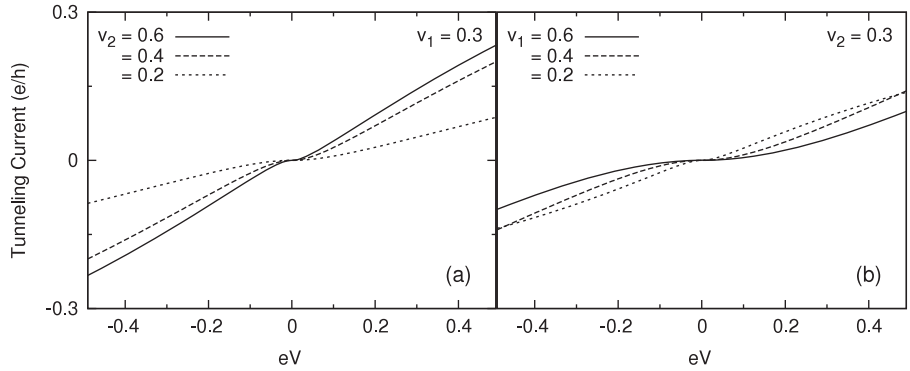

Figure 6. The I–V characteristics of the system, at low temperature. Since the parameters of the system are all set equal, the curves in (a) and (b) correspond to the transmission probabilities shown in figures 4 and 5, respectively.

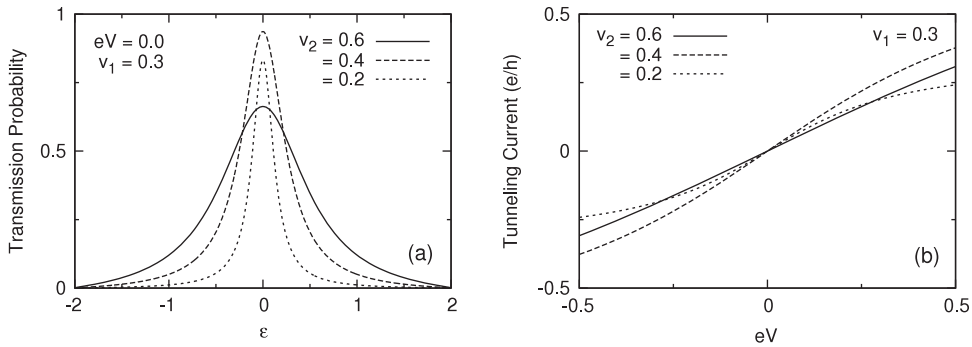

Figure 7. Examples of the graphs of (a) the transmission probability and (b) the tunneling current of the imaginary 1D–dot–1D system.

more reminiscent of those of $|G^r_{11}(\varepsilon)|^2$: a simple peak around $\varepsilon = 0.0$ (not shown). This expectation is seen to be best fulfilled at non-zero bias, as in figures 4(b)–(d).

As eV is increased from zero to higher values, from figures 4(a)–(d), the anti-resonant dip moves to the left under the control of equation (26); the two peaks shift also to the

left, accordingly. What is noteworthy here is that the left (right) peak diminishes (grows) monotonically with increasing eV. This behavior is to some extent understandable because we already know that a non-zero bias breaks the symmetry of $\mathcal{T}(\varepsilon, V)$. A more concrete accounting for this issue comes from the potential profile that we use. Referring to figure 1(b), as we increase eV, the energy-band diagram of the 1D (2D) part goes up (down), with $\varepsilon_c = 0.0$, the (unbroadened) on-site energy of the central site, kept fixed. As a result, the system possesses a wider filled energy range on the 1D source part for the incoming electron, while a wider empty energy range on the 2D drain part for the outgoing electron. We remember also that the on-site energy of the central site is actually broadened due to its coupling to the 1D and 2D parts (but it is still centered around $\varepsilon = \varepsilon_c = 0.0$), and that the features of $\mathcal{T}(\varepsilon, V)$ are to resemble more and more a simple peak around $\varepsilon = 0.0$, as we stressed above. All these factors come together to culminate in a transmission probability which, as eV is increased to more positive values, tries more and more to locate itself around $\varepsilon = 0.0$, with an amplitude more and more pronounced simultaneously. If we now take also equation (26) into account, we see that all the transmission probability graphs in figure 4 have actually a single peak with its left side cleaved at the foot. In other words, the two peaks originate from the single energy level of the central site.

To sum up, the effect of the 2D graphene part on the system is always noticeable: in all graphs, irrespective of the v_2-values and the applied bias voltage, this effect always comes into play by dividing the main original transmission peak into two, and by so creating an anti-resonant dip. Although this effect seems to diminish at high eV values of interest within the given energy band, like the one in figure 4(d), it is still easily discernible, hence significant.

The system, with a single central site, considered in the present work might be seen to mimic a simple model to study an STM system which is composed of the 1D part as the tip, the 2D graphene part as the surface, and the single central site as an adatom on the surface. We have investigated in a previous work [13] such a similar system in which we have considered a quasi-2D electron gas, imitating a metal surface via a confining potential perpendicular to the surface, instead of the 2D graphene part of the present work. In that work we focused on the bound state which appeared at the energy slightly below the surface-state low band edge; the origin of the bound state was the coupling between the central site and the quasi-2D part. In the present work there exists no such bound state since the graphene part is purely 2D, without any impurity; we do not contemplate any confining potential here. In an STM experiment, the transmission properties of interest can be attained mainly from the variation of the LDOS of the adatom by controlling the position of the tip probe or changing the voltage bias. In this sense, the coupling between the 1D tip and the adatom seems to be more meaningful than that between the adatom and the 2D graphene. (This does not lessen the importance of the 2D graphene, however.) As was also demonstrated in the previous work [13], we shall shortly see that the coupling between the 1D tip and the adatom (i.e. the single central site), too, imposes substantial effects on the system.

To investigate the role of the 1D part on the system, in figure 5 are plotted the graphs of $\mathcal{T}(\varepsilon, V)$ for several v_1 values. We keep v_2 fixed so that the effect of the 2D graphene part can be safely said to remain constant. All the general features of the previous case are also markedly distinguished here: the symmetric transmission probability at zero bias in figure 5(a), and the asymmetry caused then by a non-zero bias in figures 5(b)–(d), and the anti-resonant dip between the two peaks with its location ruled by equation (26).

At zero voltage bias, the inset in figure 5(a), we see that the heights of the two symmetric peaks are not influenced so much by the change in the hopping energy v_1 between the 1D and central site, no matter how big this change is. This situation is different in its counterpart shown in the inset in figure 4 (a), where the heights of the two peaks increase with the increasing v_2-value. Another discrepancy between figures 4 and 5 is that, for a non-zero bias voltage eV, the transmission probability graphs in the latter cross each other and intertwine unlike the case in the former where, although a small level crossing is seen, the graphs are not intertwined. We note that the graphs in figure 4 are highly height-ordered according to the v_2-values both on the left and the right sides, whereas as in figure 5 the height order on the left side is completely opposite to that on the right side. It is fairly difficult to determine the v_1 and v_2 effects analytically on the heights, crossings, height-ordering, and even positions of the two peaks from $\mathcal{T}(\varepsilon, V)$, equation (23), because of its intrinsic complex structure coming especially from the 2D graphene part. Hence, we do not resort to an analytical analysis, and are content with the numerical results with the aim of drawing the attention of the reader to the fact that the individual effects of v_1 and v_2 (i.e. those of the 1D and 2D graphene parts) on the system are of different natures.

At a given voltage bias, as the 1D part–central site coupling is strengthened by increasing the v_1-value, the height of the right peak reduces while that of the left one increases, as seen in figures 5(b)–(d). The positions of the two peaks seem dependent fairly strongly on the v_1-value; in the corresponding situation in figure 4, a v_2-dependent peak position is hardly noticeable. We see again in figures 5(b)–(d) that the changes in the heights of the left and right peaks are not at the same rate at a fixed bias. We notice also here that the right peak is favored with broader and higher features compared to the left peak; this is expected because the point $\varepsilon = 0.0$, that is the original place of the on-site energy of the central site, is on the right. This is best seen in higher eV values, e.g. figure 5(d).

As to the individual effect of increasing eV, figures 5(a)–(d), we observe very similar characteristics to the previous case: the anti-resonant dip and the two peaks move again to the left because of equation (26), and the right (left) peak grows (diminishes) monotonically with increasing eV. All these result from the interplay between the potential profile and the (broadened) eigenenergy of the central site around $\varepsilon = \varepsilon_c = 0.0$. As eV increases, the transmission probability is located closely around $\varepsilon = 0.0$, with its pronounced amplitude at the same time.

We have come to the I–V characteristics of the system. In order to best appreciate the function of the 2D graphene

part, we include in the discussion the hypothetical 1D–dot–1D system which is obtained by replacing the 2D graphene part of the present system with a 1D right lead identical to the left one; we give in figure 7 the related transmission probability and I–V graphs of this system. The notable features are the Lorentzian-shaped transmission probability curves centered around $\varepsilon = 0.0$ and the symmetric I–V curves.

We display the I–V characteristics of the present system in figure 6. There appear two important differences between the 1D–dot–1D and 1D–dot–graphene systems. The most noticeable one is that the current for a specific parameter setting in the latter is smaller than the corresponding one in the former. The discrepancy in the currents between figures 6(a) and 7(b) is small, but significant, and that between figures 6(b) and 7(b) is remarkably big. The clue to this situation comes from figures 4 and 5, where the heights and widths of the $\mathcal{T}(\varepsilon, V)$ curves, of the 1D–dot–graphene system, are much smaller than those of the 1D–dot–1D system; an example for the zero-bias case is shown in figure 7(a). In other words, in passing from the 1D–dot–1D to the 1D–dot–graphene system, the central resonant transmission peak is largely destroyed, being reshaped mostly by the 2D graphene part. Recalling that the current at sufficiently low temperature is simply the area under the transmission probability curve, equation (21), it is then natural to end up with such smaller currents. The destruction in the transmission probability curves is especially prominent in figure 5; consequently, the current shown in figure 6(b) is much smaller than that in figure 6(a), both of which are to be compared with that in the 1D–dot–1D system in figure 7(b).

The second important difference between the 1D–dot–1D and 1D–dot–graphene systems is that we witness in the latter an almost *flat*, practically zero-current region on a rather big bias interval, centered around $eV = 0.0$. The appearance of this zero-current region is totally unexpected, for its existence cannot be anticipated, even with the help of the transmission probability curves and the potential profile which we are using; we say more on this in the following.

There are some features which are common to the both cases considered in figure 6. As expected, the $I(V)$ curves are symmetric, i.e., $I(-V) = -I(V)$, so that it is enough in the following, whenever necessary, to discuss only the positive-eV part. Although they in general exhibit nonlinear behavior, within the band (of the 1D part) of interest and the small voltage bias considered, the current curves might be safely said to be linear most of the time. They are generally composed of three distinct parts: the almost linear parts in the interval $-0.5 < eV < -V_t$ and $V_t < eV < 0.5$, and between them the flat, almost zero-current region. Here we have introduced $V_t > 0$ as the *threshold voltage*; whenever V_t is reached from smaller values, for example, the current starts to increase suddenly, accommodates itself rather quickly to assume a new slope, and then continues linearly. The threshold voltage V_t for the system considered in figure 6(a) does not seem strongly dependent on the v_2-value. For the system in figure 6(b), V_t appears, on the other hand, dependent on the v_1-value; the higher v_1, the wider the zero-current interval.

Figure 6(a) displays the v_2-dependence of the current corresponding to the transmission probabilities shown in figure 4. In order to understand the reason for the almost zero-current behavior, we take a closer look at the positions of the two transmission probability peaks, and remember that the current at a specific bias voltage is simply the area under the $\mathcal{T}(\varepsilon, V)$-curve over the interval $[-eV/2, eV/2]$. When $eV < V_t$, the two peaks of $\mathcal{T}(\varepsilon, V)$ are largely outside the integral range, resulting in an almost zero current. As eV increases, the right peak, which is much broader than the left one, starts to shift to the left so that it enters seemingly suddenly the integral range $[-eV/2, eV/2]$, as seen in figure 4. (The reader is to note that it is only the right peak that contributes to the current; the left one is always outside the integral range, for, of course, the positive bias cases.) The result is an abrupt and drastic increase in the current. The magnitude of the resultant current depends on the v_2-value; the higher v_2, the bigger the current. This should be obvious from the transmission probability curves in figure 4: the higher v_2, the bigger the area under the $\mathcal{T}(\varepsilon, V)$-curve (due to the right peak).

The v_1-dependence of the current corresponding to the transmission probabilities shown in figure 5 is presented in figure 6(b). In this case, because the position of the right transmission probability peak depends more strongly on v_1 compared to the counterpart previous v_2-dependence, the magnitude and the shape of the current curve are distinctly different; the higher v_1, the smaller the current, within the range of voltage bias of interest. The seeming linearity seen in the previous case is not so 'literal' in this case. The reason for the flat, zero-current range is the same as before; no need to contemplate further. As to the reason for a smaller current, it suffices to note from figure 5 that the area under the right peak of the transmission probability curve is somewhat smaller than the corresponding previous case. Lastly, as v_1 is decreased, with v_2 kept fixed, the threshold voltage V_t becomes smaller and smaller since the width of the right transmission peak gets narrower, making the zero-current interval narrower, also. We note, again, that although in this case the left transmission peak appears to possess a broad feature, like the right one, it contributes nothing to the current.

Before closing it seems in order to mention a subtle point. In this work the 2D graphene part occupies the central part because of its inherent zero-gap band structure around a K-point. It is well known that both the static and dynamic dielectric functions of a pure zero-gap superconductor have singularities at zero temperature [21]. These singularities are especially important under electromagnetic fields. To our best knowledge there is no study probing similar situations in 2D cases, notably in the 2D graphene (we are not talking about carbon nanotubes). Our study completely excludes the possibility of such singularities in graphene. If such singularities happen to exist in graphene, the results of the present work will certainly be affected, but, nevertheless, they might be used as markers for probing comparatively the effects of the presence of singularities.

In this work we study the electron transport problem in a 1D–dot–2D-graphene system to find out its transmission properties and I–V characteristics. Three important analytical properties of the system seem to prevail: $\mathcal{T}(-\varepsilon, -V) = \mathcal{T}(\varepsilon, V)$, $\mathcal{T}(-eV/2, V) = 0$, and $I(-V) = -I(V)$. In

all $\mathcal{T}(\varepsilon, V)$ graphs there appear two peaks, together with a zero-transmission dip between them. All the $\mathcal{T}(\varepsilon, V)$-graphs possess in fact a single central transmission peak, due originally to the single energy level of the central site, with its left side cleaved at the foot. The destruction of the transmission peak, leading to a small current, is a sheer effect of the 2D graphene part. The I–V graphs of the 1D–dot–graphene system always have an almost flat, practically zero-current region on a rather big bias interval, a totally unexpected result not seen in the 1D–dot–1D system. The almost zero-current region results from the interplay between the applied bias voltage, together with the bias profile used, and the two transmission peaks. It is owing to the flat region, with the two linear regions on two sides, that in a real application the device proposed in this work might be used as a one-way conventional diode, or a two-way Zener diode. We see that only one of the two transmission peaks contributes to the current, a property that seems important in manipulating the system at hand to accommodate it according to particular needs. The present work may be improved for the case in which a chain of atomic sites or dots can be replaced with the single site of the present system. The result would be a new system having more transmission probability peaks. Since the graphene part will now cause the device to act as some kind of 'transmission-peak shifter', the thus-obtained device might be easily engineered in choosing which transmission peak(s) will contribute to the current by modulating the on-site potentials of the central chain and by changing the applied voltage; nevertheless, whether such a device practically works as a promising device is not the issue of this work.

Acknowledgments

The authors gratefully acknowledge invaluable discussions with Wonmyung Woo and Dongkwan Shin. This work was supported by the Korea Research Foundation, grant no KRF-2006-0409-0060.

References

[1] Wallace P R 1947 *Phys. Rev.* **71** 622
[2] Saito R, Dresselhaus G and Dresselhaus M S 1998 *Physical Properties of Carbon Nanotubes* (London: Imperial)
[3] Novoselov K S, Geim A K, Morozov S V, Jiang D, Zhang Y, Dubonos S V, Grigorieva I V and Firsov A A 2004 *Science* **306** 666
[4] Novoselov K S, Jiang D, Schedin F, Booth T J, Khotkevich V V, Morozov S V and Geim A K 2005 *Proc. Natl Acad. Sci. USA* **102** 10451
[5] Novoselov K S, Geim A K, Morozov S V, Jiang D, Katsnelson M I, Grigorieva I V, Dubonos S V and Firsov A A 2005 *Nature* **438** 197
[6] Zhang Y, Tan Y, Stormer H L and Kim P 2005 *Nature* **438** 201
[7] Isihara A 1993 *Electron Liquids* (Berlin: Springer)
[8] Berger C, Song Z, Li T, Li X, Ogbazghi Y, Feng R, Dai Z, Marchenkov A N, Conrad E H, First P N and Heer W A 2004 *J. Phys. Chem.* B **108** 19912
[9] Ohta T, Bostwick A, Seyller T, Horn K and Rotenberg E 2006 *Science* **313** 951
[10] Stankovich S, Dikin D A, Dommett G H, Kohlhaas K M, Zimney E J, Stach E A, Piner R D, Nguyen S T and Ruoff R S 2006 *Nature* **442** 282
[11] Caroli C, Combescot R, Nozieres P and Saint-James D 1971 *J. Phys. C: Solid State Phys.* **4** 916
[12] Keldysh L V 1964 *Zh. Eksp. Teor. Fiz.* **47** 1515
Keldysh L V 1965 *Sov. Phys.—JETP* **20** 1018 (Engl. Transl.)
[13] Fukuda T, Oymak H and Hong J 2007 *Phys. Rev.* B **75** 195428
[14] Anderson P W 1961 *Phys. Rev.* **124** 41
[15] Grimley T B 1967 *Proc. Phys. Soc. London* **90** 751
[16] Grimley T B 1967 *Proc. Phys. Soc. London* **92** 776
[17] Newns D M 1969 *Phys. Rev.* **178** 1123
[18] Wang Z F, Xiang R, Shi Q W, Yang J, Wang X, Hou J G and Chen J 2006 *Phys. Rev.* B **74** 125417
[19] Meir Y and Wingreen N S 1992 *Phys. Rev. Lett.* **68** 2512
[20] Jauho A P, Wingreen N S and Meir Y 1994 *Phys. Rev.* B **50** 5528
[21] Liu L and Tan M 1974 *Phys. Rev.* B **9** 632 and references therein